Terahertz quantum cascade laser modeling for applications in imaging, sensing, and metrology

Nikola Vuković[*a], Milan Ignjatović[a], Novak Stanojević[a,b], Mihailo Stojković[a], Nikola Basta[a], Filip Perišić[a], Aleksandar Milićević[c], Aleksandar Demić[d], Dragan Indjin[d], Jelena Radovanović[a]
[a]School of Electrical Engineering, University of Belgrade, Bulevar kralja Aleksandra 73, 11120 Belgrade, Serbia, [b]Vlatacom Institute of High Technologies, Bulevar Milutina Milankovica 5, 11070 Belgrade, Serbia, [c]Vinča Institute of Nuclear Sciences, University of Belgrade, Mike Petrovića Alasa 12-14, 11001 Belgrade, Serbia, [d]School of Electronic and Electrical Engineering, University of Leeds, Leeds, LS2 9JT, UK

ABSTRACT

In the talk we present our recent modeling results for THz frequency QCLs including electronic structure and transport calculations of exemplary GaAs-based devices, investigation of alternative material platforms based on wide-bandgap semiconductors, modeling passive mode-locking with saturable absorber, and study of optical feedback effects. Moreover, we employ a machine learning framework for THz QCL design optimization. Methods include a Schrödinger-Poisson solver for calculating eigenenergies and wave functions, a density matrix carrier transport model, Maxwell-Bloch equations for passive mode-locking and self-mixing dynamics, and a multi-layer perceptron neural network to predict the laser transition figure of merit.

Keywords: THz quantum cascade laser, transfer matrix method, density matrix transport model, wide-bandgap semiconductors, Maxwell-Bloch equations, passive mode-locking, neural network

1. INTRODUCTION

Terahertz (THz) frequency quantum cascade lasers (QCLs) have remarkably improved since the first demonstration [1] in terms of optical bandwidth, optical power levels, and spectral purity, representing an enabling quantum technology with the potential of bridging the dead zone between electronics and optics, the so-called THz technology gap [2]. Namely, it opens fascinating perspectives in quantum science with an impact on all main areas, from sensing and metrology to communication, computation, and simulation [3], [4]. Non-ionizing THz radiation is suitable for medical imaging and studying cellular and molecular biology. However, for further advances in the field, the reduction of the cost and complexity of THz spectroscopy and imaging systems are desirable and this can be achieved by using high-performance computing and machine learning techniques [5] for designing higher power sources with near room temperature operation, sources of ultra-short and high-intensity THz pulses [6], as well as more sensitive detectors. Furthermore, self-mixing with the THz QCL is a fast and sensitive technique that removes the need for an external THz detector, which is essential for emerging applications ranging from imaging of human skin pathologies [7] to the hydration sensing of leaves [8].

2. METHODS

We calculate QCL electronic structures by solving the Schrödinger equation within the electron effective mass formalism using the derivative transfer matrix method (dTMM) developed in [9]. Depending on the underlying material systems and crystal structure, the solutions deviate from parabolic dispersion and require treatment of nonparabolicity, especially in semiconductor structures with small bandgaps and multiple quantum well (MQW) systems, which comprise narrow energy spacing between the subbands, as well as MQW systems possessing high-energy subbands. The most common approaches for the calculation of the nonparabolicity effects in the conduction band are the two-band Kane model, which takes into account the interaction of the conduction band and the light-hole valence band, and a more complex treatment that uses a 14-band $\mathbf{k}\cdot\mathbf{p}$ model [10].

[*] nvukovic@etf.bg.ac.rs

Optical Methods for Inspection, Characterization, and Imaging of Biomaterials VII, edited by Pietro Ferraro
Simonetta Grilli, Demetri Psaltis, Andreas E. Vasdekis, Proc. of SPIE Vol. 13571, 135711R
2025 Published by SPIE · 0277-786X · doi: 10.1117/12.3068611

The density matrix (DM) quantum transport model, which we use, was developed in [11], [12]. It employs the first neighbor and tight binding approximations, together with the infinite period QCL consideration. It is a multipurpose model with low numerical complexity that incorporates coherence effects and accurately describes resonant tunneling through the injection barrier, making it excellent for the intensive optimization of THz QCL structures in high-performance computing facilities. All of the scattering mechanisms of interest are described as perturbations with Fermi's golden rule.

For modeling QCL active region dynamics, we use macroscopic Maxwell–Bloch (MB) equations, a widely used semiclassical model to describe optical propagation and coherent light–matter interaction in media consisting of discrete-level quantum systems [13]. We study the pulse formation in a bound-to-continuum (BTC) QCL from [14] operating at ~3 THz, with a graphene saturable absorber (SA) stripes, which exhibited passive mode locking in an experiment in [6]. Our time-domain simulations are performed on a system with eleven quantized energy states, and we apply rotating wave approximation (RWA) and slowly varying envelope approximations (SVEA). We also compare results with our 2-level full-wave model with SA and the 2-level model from [15] which uses RWA and SWEA.

We perform time-domain simulations of a 2 THz BTC QCL design [11] in laser feedback interferometry (LFI) configuration, by adopting effective semiconductor Maxwell-Bloch equations approach from [16]. Parameters for self-mixing simulations are extracted from the DM transport model.

Finally, we use a multi-layer perceptron (MLP) neural network to predict the laser gain, current density, and frequency of ~175 thousand QCL designs using layer thicknesses and the applied electric field as inputs, following the approach from [5]. The reference QCL is a record-high-temperature 2-well design reported in [17].

3. RESULTS

In this Section we present a portion of the numerical results which are presented during the talk and available on the presentation, namely time-domain simulations of QCL with SA and prediction of transport parameters using MLP.

Figure 1 shows conduction band profile and squared wavefunctions obtained by self-consistently solving the Schrödinger–Poisson system. Design is from reference [14] and it was used in an experiment in which passive mode-locking was demonstrated in THz QCL for the first time [6].

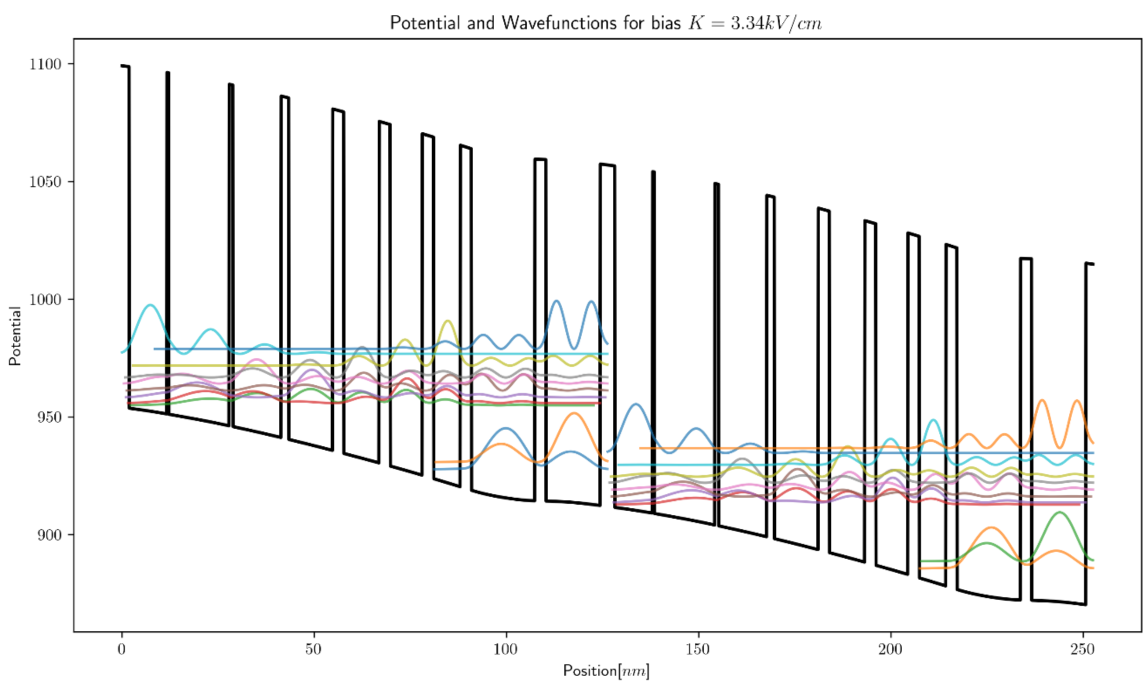

Figure 1. Conduction band potential of the 3 THz BTC THz QCL, along with moduli squared of the corresponding wave functions [14]. The figure shows two adjacent active regions.

We calculate transport parameters (gain, current density, and peak gain frequency) using the DM transport model, and extract eigen energies, dipole moments, wavefunctions and all the scattering rates for subsequent time-domain simulations.

Then, we numerically solve the MB equations in RWA and SVEA for the 11 states shown in Fig. 1. The graphene saturable absorber is modeled as a slow absorber, as in [6]. Intensity waveform and its spectrum are plotted in Figs. 2 and 3, respectively. Results show good agreement with the experiment [6] in terms of pulse width (~4 ps) and optical spectrum shape around 3 THz, and also with numerical simulations reported in [6] for 9 states. We can also generate similar waveforms and output power spectra using simplified 2-level models with or without RWA and SVEA. However, this simplification is artificial; it requires fitting of parameters to the model with N>2 states and, although it catches the mode-locking dynamics with graphene saturable absorber, it is in our opinion necessary to consider all of the 11 states in the simulation to correctly catch all the dynamic peculiarities. Nevertheless, the larger the number of states considered in the simulation, the larger the number of equations and consequently the execution time of the time-domain simulations over several thousands of round trips.

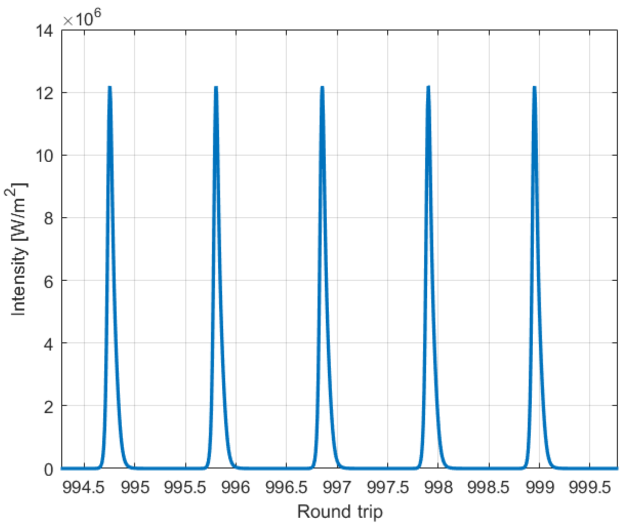

Figure 2. Intensity waveform from a QCL in Fig. 1 with distributed graphene saturable absorber. Pulses are ~4 ps wide in agreement with the experiment reported in [6]. In simulation we use group velocity dispersion value $\beta_2=10^{-22}\ s^2m^{-1}$.

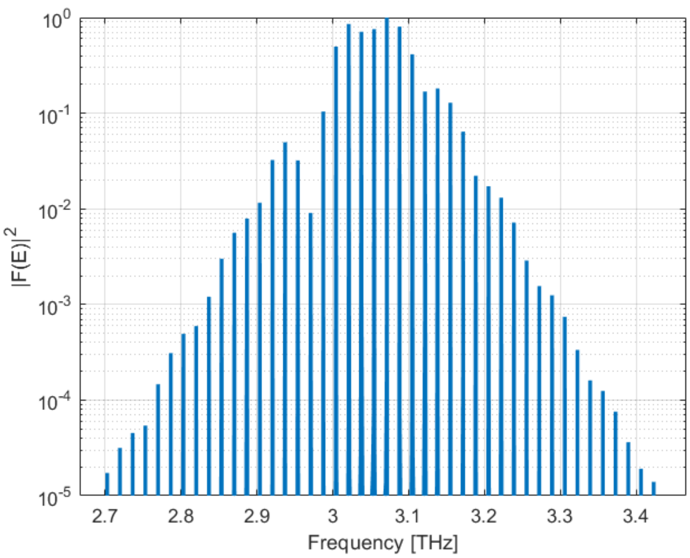

Figure 3. Normalized optical power spectra that correspond to the intensity waveform shown in Fig. 2.

In the following, we show numerical results of MLP neural network, which was used to search for the optimal structures around the reference design from the literature [17] The dataset is divided into 80% random configurations for training and 20% for testing. We use a batch size of 32, as a loss function, we use mean square error and L2 regularization, Adam optimizer with a learning rate of 0.001, and 300 epochs. MLP architecture consists of the input layer, three hidden layers and the output layer. The input layer has 7 values (6 material layer widths and external electric field). Each material layer is varied around the reference value by ±2 monolayers with one monolayer thickness step, while the electric field is varied from 17.5 to 27.5 kV/cm with a 2 kV/cm step. First hidden layer has 7 inputs and 64 outputs, PReLU activation function. Second hidden layer has 64 inputs and 128 outputs, PReLU activation function. The third hidden layer has 128 inputs and 64 outputs. Figures 4, 5 and 6 show a comparison between the predicted and the results from the QCL simulator (actual) for material gain, current density, and peak gain frequency, respectively. Figure 7 shows how the loss function evolves with the number of epochs.

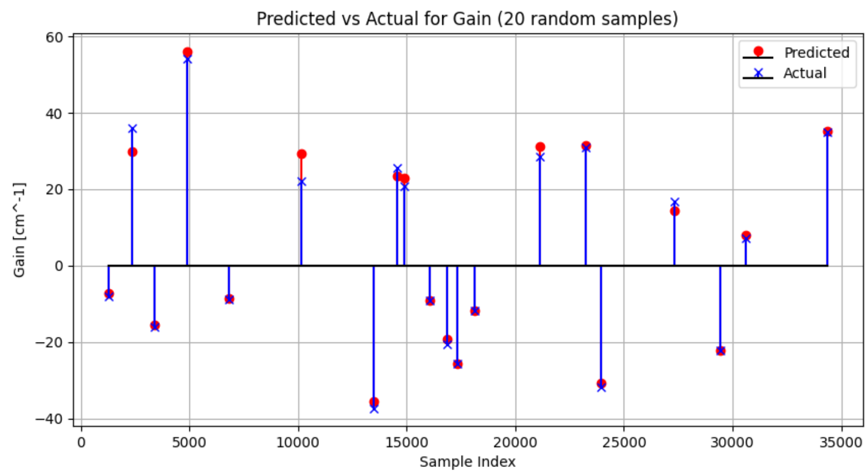

Figure 4. Results of our MLP neural network trained to predict material gain. On 20 random samples, we show a comparison between the predicted (MLP) and the results from the QCL simulator (actual) employing DM quantum transport [11], [12]. Reference structure is 261 K 2-well design [17].

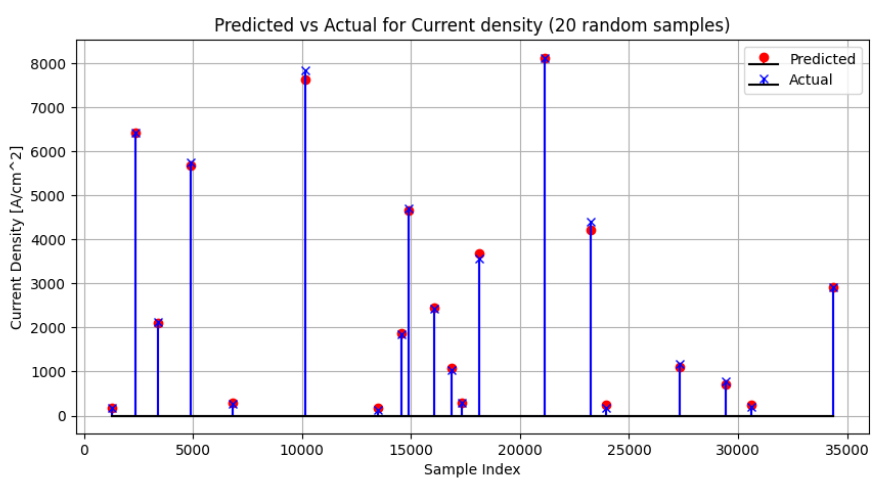

Figure 5. Results of our MLP neural network trained to predict current density. On 20 random samples, we show a comparison between the predicted (MLP) and the results from the QCL simulator (actual) employing DM quantum transport [11], [12]. Reference structure is 261 K 2-well design [17].

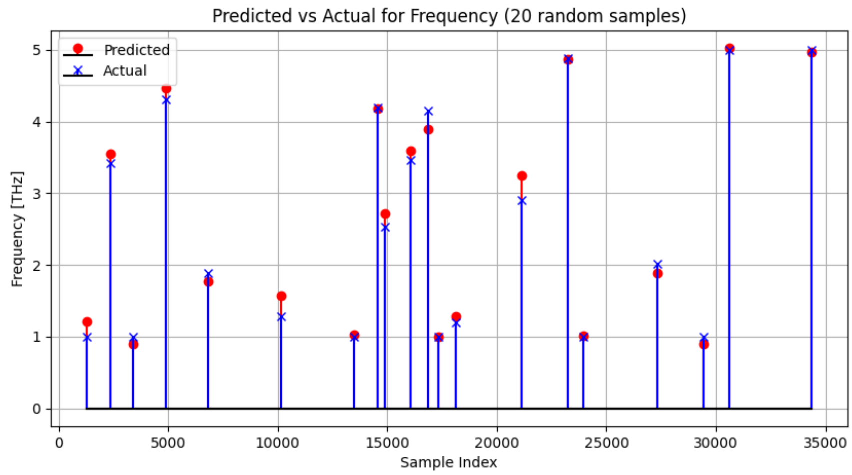

Figure 6. Results of our MLP neural network trained to predict THz QCL operating frequency. On 20 random samples, we show a comparison between the predicted (MLP) and the results from the QCL simulator (actual) employing DM quantum transport [11], [12]. Reference structure is 261 K 2-well design [17].

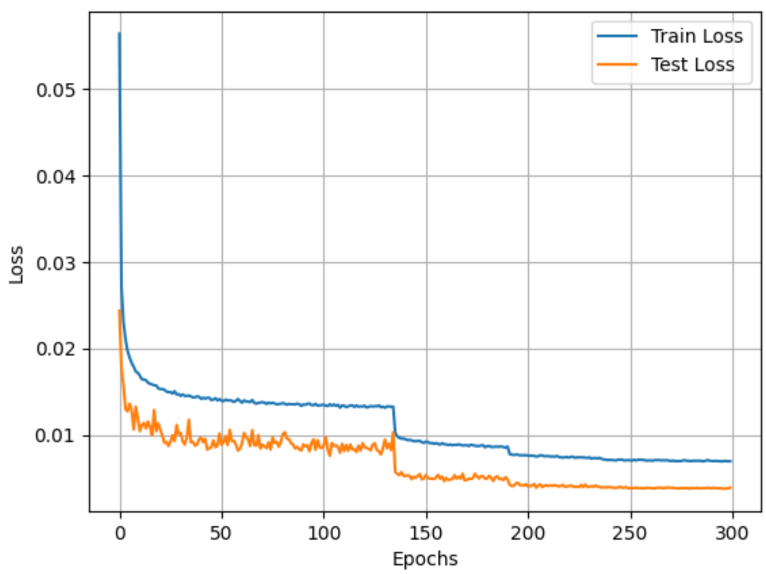

Figure 7. Loss function (mean square error and L2 regularization) as a function of the number of epochs.

4. CONCLUSION

To conclude, in this talk, we have presented our recent modeling results for terahertz frequency quantum cascade lasers, devices with applications in imaging, sensing, and metrology. These results include electronic structure and transport calculations, time-domain simulations, and optical spectra of intensity waveforms, as well as the application of a neural network for predicting transport parameters.

ACKNOWLEDGEMENTS

This work was financially supported by the Science Fund of the Republic of Serbia, 10504, "Ultra-short pulsations from TERAhertz quantum cascade laser using passive mode-LOCKing with graphene saturable absorber" – TERALOCK, Ministry of Science, Technological Development and Innovation of the Republic of Serbia under contract number: 451-03-137/2025-03/200103, COST Action CA21159 PhoBioS, and Vlatacom Institute of High Technologies under project 178.

REFERENCES

[1] R. Köhler *et al.*, "Terahertz semiconductor-heterostructure laser," *Nature*, vol. 417, no. 6885, pp. 156–159, May 2002, doi: 10.1038/417156a.

[2] M. S. Vitiello and A. Tredicucci, "Physics and technology of Terahertz quantum cascade lasers," *Adv Phys X*, vol. 6, no. 1, Jan. 2021, doi: 10.1080/23746149.2021.1893809.

[3] G. Scalari and J. Faist, "30 years of the quantum cascade laser," *Commun Phys*, vol. 7, no. 1, p. 394, Dec. 2024, doi: 10.1038/s42005-024-01888-z.

[4] D. Botez and M. A. Belkin, Eds., *Mid-Infrared and Terahertz Quantum Cascade Lasers*. Cambridge University Press, 2023. doi: 10.1017/9781108552066.

[5] A. Correa Hernandez and C. F. Gmachl, "A machine learning framework for quantum cascade laser design," *APL Machine Learning*, vol. 2, no. 3, Sep. 2024, doi: 10.1063/5.0222812.

[6] E. Riccardi *et al.*, "Short pulse generation from a graphene-coupled passively mode-locked terahertz laser," *Nat Photonics*, Apr. 2023, doi: 10.1038/s41566-023-01195-z.

[7] X. Qi *et al.*, "Terahertz imaging of human skin pathologies using laser feedback interferometry with quantum cascade lasers," *Biomed Opt Express*, vol. 14, no. 4, p. 1393, Apr. 2023, doi: 10.1364/BOE.480615.

[8] K. Singh *et al.*, "Comparison of Physical and System Factors Impacting Hydration Sensing in Leaves Using Terahertz Time-Domain and Quantum Cascade Laser Feedback Interferometry Imaging," *Sensors*, vol. 23, no. 5, p. 2721, Mar. 2023, doi: 10.3390/s23052721.

[9] N. Stanojević *et al.*, "Derivative transfer matrix method: Machine precision calculation of electron structure and interface phonon dispersion in semiconductor heterostructures," *Comput Phys Commun*, vol. 311, p. 109573, Jun. 2025, doi: 10.1016/j.cpc.2025.109573.

[10] U. Ekenberg, "Nonparabolicity effects in a quantum well: Sublevel shift, parallel mass, and Landau levels," *Phys Rev B*, vol. 40, no. 11, pp. 7714–7726, Oct. 1989, doi: 10.1103/PhysRevB.40.7714.

[11] A. Demic *et al.*, "Infinite-Period Density-Matrix Model for Terahertz-Frequency Quantum Cascade Lasers," *IEEE Trans Terahertz Sci Technol*, vol. 7, no. 4, pp. 368–377, Jul. 2017, doi: 10.1109/TTHZ.2017.2705481.

[12] A. Demić, Z. Ikonić, R. W. Kelsall, and D. Indjin, "Density matrix superoperator for periodic quantum systems and its application to quantum cascade laser structures," *AIP Adv*, vol. 9, no. 9, Sep. 2019, doi: 10.1063/1.5095246.

[13] C. Jirauschek, M. Riesch, and P. Tzenov, "Optoelectronic Device Simulations Based on Macroscopic Maxwell–Bloch Equations," *Adv Theory Simul*, vol. 2, no. 8, Aug. 2019, doi: 10.1002/adts.201900018.

[14] L. H. Li *et al.*, "Broadband heterogeneous terahertz frequency quantum cascade laser," *Electron Lett*, vol. 54, no. 21, pp. 1229–1231, Oct. 2018, doi: 10.1049/el.2018.6062.

[15] L. Seitner, J. Popp, M. Haider, S. S. Dhillon, M. S. Vitiello, and C. Jirauschek, "Theoretical model of passive mode-locking in terahertz quantum cascade lasers with distributed saturable absorbers," *Nanophotonics*, vol. 13, no. 10, pp. 1823–1834, Apr. 2024, doi: 10.1515/nanoph-2023-0657.

[16] C. Silvestri, L. L. Columbo, M. Brambilla, and M. Gioannini, "Coherent multi-mode dynamics in a quantum cascade laser: amplitude- and frequency-modulated optical frequency combs," *Opt Express*, vol. 28, no. 16, p. 23846, Aug. 2020, doi: 10.1364/OE.396481.

[17] A. Khalatpour, M. C. Tam, S. J. Addamane, J. Reno, Z. Wasilewski, and Q. Hu, "Enhanced operating temperature in terahertz quantum cascade lasers based on direct phonon depopulation," *Appl Phys Lett*, vol. 122, no. 16, Apr. 2023, doi: 10.1063/5.0144705.